Fundamental Research 1 (2021) 684–690

Contents lists available at ScienceDirect

Fundamental Research

journal homepage: http://www.keaipublishing.com/en/journals/fundamental-research/

Article

Low-threshold wavelength-tunable ultraviolet vertical-cavity surface-emitting lasers from 376 to 409 nm

Yang Mei, Tian-Rui Yang, Wei Ou, Zhong-Ming Zheng, Hao Long, Lei-Ying Ying, Bao-Ping Zhang*

Department of Microelectronics and Integrated Circuits, Laboratory of Micro/Nano-Optoelectronics, School of Electronic Science and Engineering, Xiamen University, Xiamen 361005, China

ARTICLE INFO

Article history:
Received 5 July 2021
Received in revised form 23 October 2021
Accepted 1 November 2021
Available online 14 November 2021

Keywords:
UVA VCSELs
Wavelength-tunable
Wedge-shaped cavity
Resonant period gain

ABSTRACT

Optically pumped wavelength-tunable vertical-cavity surface-emitting lasers (VCSELs) operating in the ultraviolet A (UVA) spectrum were demonstrated. The VCSELs feature double dielectric distributed brag reflectors and a wedge-shaped cavity fabricated using the substrate transfer technique and laser lift off, resulting in a graded cavity length in one device. A resonant period gain structure is used in the InGaN/GaN multi-quantum well active region to enhance the coupling between the cavity mode field and the active layers. The optical field inside the cavity is modulated by the cavity length; thus, tunable lasing at different wavelengths is realized at different points of a single VCSEL chip. The lasing wavelength extends from 376 to 409 nm, covering most of the UVA band below the band gap of GaN. The threshold pumping power density of the UVA VCSELs at different wavelengths ranges from 383 to 466 kW/cm^2, which is among the lowest values for ultraviolet (UV) VCSELs. This study is promising for the development of small-footprint, power-efficient UV light sources.

1. Introduction

Vertical-cavity surface-emitting lasers (VCSELs) have circular and low-divergent output beams, low threshold currents, high modulation rates, 2D-array manufacturability, and compatibility with on-wafer testing [1,2]. These advantages make VCSELs suitable for a variety of practical applications compared with other types of light sources such as light-emitting diode (LED) and edge-emitting lasers (EELs). With their small cavities and strong optical confinement, VCSELs are also important in fundamental studies such as cavity quantum electrodynamics (CQED) [3,4]. After decades of development, GaAs-based infrared VCSELs have dominated the market in short-reach data communication since commercialization [5], and are further boosted by increasing demand for 3D sensing applications such as face recognition and automatic pilot [6]. The success of GaAs-based VCSELs has promoted the development of its short-wavelength counterparts, visible and ultraviolet VCSELs. To fabricate VCSELs in the visible and ultraviolet regions, III-nitride materials including InGaN, GaN, AlGaN, and AlN are ideal choices for their wide and tunable direct energy gaps [7,8]. The first electrically injected III-nitride-based blue VCSEL was produced in 2008 [9]. With continued research and commitment, the performance of visible VCSELs has improved significantly in recent years. The emission wavelengths of electrically injected III-nitride-based VCSELs extend from 405–565 nm [10–25], and the output powers of single diodes and device arrays have reached 24 mW [26] and 1 W [14], respectively. The wall plug efficiencies were approximately 10%, approaching the practical level. In 2021, Nichia Corporation reported yields of more than 80% over a 2-inch wafer, and 1000 h continuous operation at room temperature for blue VCSELs [27]. These results suggest the upcoming commercialization of visible III-nitride-based VCSELs, which is expected to greatly promote development of full-color pico-projectors and wearable electronics such as retinal scanning displays for augmented and virtual reality [28].

With the progress made in visible III-nitride-based VCSELs, attention has now turned to UV VCSELs at wavelengths below 400 nm for their tremendous potential in certain applications. The UV wavelength range can be further subdivided into four bands: long-wave ultraviolet UVA (315–400 nm), medium-wave ultraviolet UVB (280–315 nm), short-wave ultraviolet UVC (200–280 nm), and vacuum ultraviolet (100–200 nm) [29]. In principle, III-nitride-based VCSELs can be made with emission wavelengths covering most of the UV spectrum, as the band gap of AlN can reach 6.2 eV [30]. The potential applications of UV VCSELs are mainly dependent on the emission band. UVA VCSELs serve as the primary light source in the curing of UV glue, light therapy, air purification, and 3D printing [29]. UVA VCSELs with an emission wavelength of 369 nm are crucial for realization of next-generation compact ytterbium-ion-based atomic clocks [31]. UVA VCSELs can also be used as a light source for luring lamps because many insects show intense positive phototaxis in UVA [32]. The main application of UVB and UVC VCSELs is probably disinfection of water and surfaces [33–35]. These emission bands correspond to peaks in the absorption spectra of DNA and RNA. Exposure

* Corresponding author.
E-mail address: bzhang@xmu.edu.cn (B.-P. Zhang).

https://doi.org/10.1016/j.fmre.2021.11.001

of bacteria and viruses to UVB/C light causes photochemical changes in genetic materials, inducing the loss of self-replicating ability. UVB/C VCSELs can also be used in sensing [36], lithography [37], and medical and agricultural applications [38]. These applications may also be satisfied by commercially available UV LEDs, but VCSELs would provide additional benefits such as small size, low power consumption, higher irradiance, more directional output beams, and a combination of targeted and large-area treatment using arrays of individual addressable devices.

Compared with visible VCSELs, the development of UV VCSELs is more challenging and there is still no electrically injected laser operation in the sub-400 nm region. The difficulties mainly lie in the growth of active layers with high gain in UV, fabrication of a low-loss microcavity, and realization of high-efficiency current injection. As the laser emission wavelength decreases, the growth of active layers with high crystal quality is more difficult; the spontaneous emission rate increases by $1/\lambda^3$, where λ is the wavelength, resulting in a much higher lasing threshold [39]. The growth of III-N-based DBRs with high reflectivity in the UV region is much more difficult due to limited choice in optically transparent materials with large refractive index contrasts and low absorption loss. For current injection, AlGaN with a high Al content is highly resistive; the commonly used indium tin oxide (ITO) ohm-contacting and current-spreading layer in visible VCSELs is not suitable for UV VCSELs due to its large absorption coefficient. The bandgap of ITO is below 350 nm, but it has a significant absorption tail that extends into the blue spectral regime [40]. The absorption coefficient can reach 7000 cm^{-1} at 375 nm; thus, other current injection schemes such as tunnel junctions must be developed for UV VCSELs. To date, the main progress in UV VCSELs has used an optical pumping excitation scheme. The first optically pumped UV VCSEL was produced in 1996 using a GaN bulk active layer and double $Al_{0.4}Ga_{0.6}N/Al_{0.12}Ga_{0.88}N$ epitaxial DBRs [41]. Laser emission near 363 nm was realized, with a large threshold power of 2 MW/cm^2. UVA VCSELs with both InGaN and AlInGaN MQW active regions were subsequently demonstrated by several groups, with a lasing wavelength from 349–403 nm [30,31,39,41-49]. Different cavity structures, including double dielectric DBR cavities, hybrid DBR cavities, and nanopillar-type cavities with double nitride DBRs have been developed; each has advantages and disadvantages. UVA VCSELs with epitaxial nitride DBRs have a simpler structure, but development of nitride DBRs with high reflectivity in the UV band is a great challenge. Devices with double dielectric DBRs avoid this difficulty, but the fabrication process is complicated because substrate removal and layer transfer are required. In 2020, Hjort et al. demonstrated the first UVB VCSEL lasing at 310 nm [48]. The device has an $Al_{0.6}Ga_{0.4}N$ cavity between two SiO_2/HfO_2 dielectric DBRs. The double-dielectric DBR design was realized by substrate removal using electrochemical etching. The threshold excitation power of the device reached 10 MW/cm^2. In 2021, we successfully realized the first UVC VCSEL lasing at 275.9 nm using a double SiO_2/HfO_2 dielectric DBR cavity and an $Al_{0.4}Ga_{0.6}N/Al_{0.5}Ga_{0.5}N$ MQW active region [30]. The threshold excitation power is ~1.21 MW/cm^2, with the shortest wavelength of III-nitride-based VCSELs. However, these devices can operate only at a single distinct wavelength, and the threshold excitation power is still relatively large, even in the UVA region. In this study, we report low-threshold wavelength-tunable UVA VCSELs from 376–405 nm. The device features a wedge-shaped cavity and two dielectric DBRs; the thickness of the cavity layer shows a gradual change in one device. The resonating wavelength of the cavity modes is tuned by the cavity length; lasing at different wavelengths can be controlled at different points on a single chip. This is crucial for applications such as dual-wavelength interferometry (DWI) for distance measurements, laser spectroscopy, and multi-wavelength optical recording systems in which multi-wavelength emission is required [50]. In addition, a resonant period gain (RPG) structure was used; two groups of InGaN/GaN MQWs were separated by a GaN spacing layer to ensure that the MQW groups were located at two antinodes of the standing wave pattern. Such an RPG structure can effectively increase the coupling between the active layers and the optical field inside the cavity. The threshold excitation power densities of the UVA VCSELs with RPG structure lasing at different wavelengths range from 383–466 kW/cm^2, which are among the lowest values reported for UV VCSELs.

2. Materials and methods

The epitaxial wafer used in this study was grown on a sapphire substrate using the MOCVD system. The epi-layer consists of a 30-nm GaN low-temperature nucleation layer, a 2-μm undoped GaN buffer layer, and a 2-μm n-GaN layer, followed by the InGaN/GaN MQW region, a 20-nm AlGaN electron blocking layer, a 97-nm p-GaN, and a 3-nm-n++ InGaN contacting layer. For the epitaxial wafer with RPG structure, four $In_{0.1}Ga_{0.9}N$ (3nm)/GaN (5 nm) QWs were grown and divided into two groups separated by a 70-nm GaN spacing layer. The thickness of each layer was carefully designed to ensure that the two groups of QWs were located at two adjacent antinodes of the standing wave pattern inside the cavity. For comparison, another epitaxial wafer was prepared with a normal active region; five QWs were continuously grown and the active region was designed to be located at a single antinode of the standing wave pattern. The epi-structure was intentionally designed for electrically injected UV VCSELs, such that the GaN spacing layer is doped and an n++ InGaN contacting layer is grown. Optically pumped lasing was realized; fabrication of electrically injected devices is in progress. To realize the VCSEL structure, 12.5 pairs of SiO_2/TiO_2 DBRs with a central wavelength of 400 nm and maximum reflectivity over 99.9% were deposited on the surface of the epitaxial wafer by e-beam evaporation. The wafer was flip-chip bonded to a quartz template, and the sapphire substrate was removed by laser lift-off (LLO). The LLO process was performed using a pulsed 248-nm KrF excimer laser. After LLO, chemical mechanical polishing (CMP) was used to obtain a flat cavity surface and a wedge-shaped cavity layer with gradually changing thickness. The top dielectric DBR, including seven pairs of TiO_2/SiO_2, was deposited to complete the optically pumped UVA VCSEL structure. Inhomogeneous cavity length is usually avoided in device fabrication for uniformity in device performance. In this study, the cavity length was intentionally controlled by the CMP process to exhibit a gradient change to tune the lasing wavelength at different positions on a single chip. The thickness of the cavity layer was estimated to change from ~0.5 μm to ~3 μm in a 10-mm lateral distance range, and demonstrated by a reflection-type thickness measurement setup. The schematic structure of the UVA VCSEL with a wedge-shaped cavity, the epitaxial structure with RPG, and the reflection spectra of the DBRs are illustrated in Fig. 1a–c, respectively.

As reported previously [51], a flat surface on the cavity layer is significant in realizing low-threshold lasing, due to reduced scattering loss. The scattering loss can be calculated as $S_{scatter} = D\{1 - \exp[-(\frac{4\pi\delta}{\lambda})^2]\}$, where δ is the root-mean-square (RMS) roughness of the cavity end faces, and D is a calibration coefficient defined as the ratio of the DBR reflectance when light is incident from air and p-GaN, respectively [25,52]. The morphologies of the bottom and top cavity surfaces in this study are shown in Fig. 1d and e, respectively. The as-grown bottom cavity surface in Fig. 1d shows an atomically flat morphology, on which the atomic steps can be clearly observed. The RMS is ~0.33 nm on a 2×2 μm^2 area. The roughness of the top cavity surface after CMP is even less, with an RMS of 0.29 nm, as shown in Fig. 1e. The super-flat cavity surface in this study indicates negligible scattering loss (<0.001%) during light oscillation.

3. Results and discussion

The emission spectra of the epitaxial wafers and the UVA VCSELs were measured under excitation by a CryLas FTSS-355 Q1 355-nm pulsed laser with a repetition frequency of 15 kHz and a pulse width of 1 ns. The circular excitation laser spot was focused on the surface with a diameter of 70 μm. The emission was collected from the top of

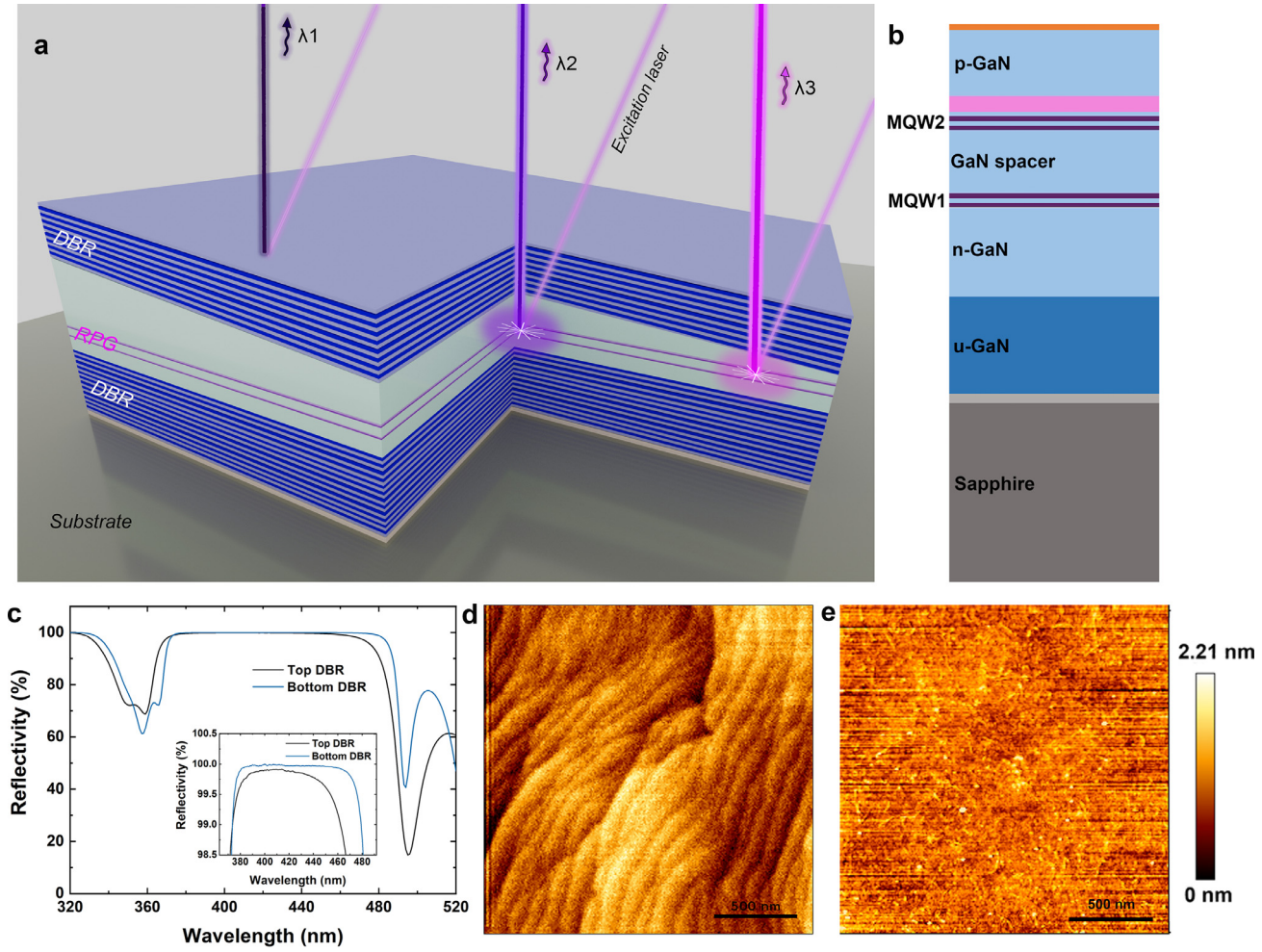

Fig. 1. Structural properties of the UVA VCSELs with wedge-shaped cavity. (a) Schematic structure of UVA VCSEL with RPG structure and wedge-shaped cavity; (b) structure of epitaxial wafer with RPG; (c) reflection spectra of top and bottom DBRs; the inset shows the enlarged spectra within the high reflection band; (d) Atomic force microscope (AFM) image of bottom cavity surface (as-grown epitaxial surface); (e) AFM image of top cavity surface (n-GaN surface after CMP).

the sample with a microscope objective (NA0.35, 10X); the light was guided through air into a monochromator with an electrically cooled charge-coupled device (CCD) as the detector. Fig. 2a shows the normalized emission spectra of the epitaxial wafers with the active regions of the normal-type and RPG structures. Both structures show a main peak centered at 400 nm emerging from the MQW active region and a small shoulder peak at ~365 nm emerging from GaN layers in the epitaxial structure. The spectra of the spontaneous emissions are modulated by the self-formed Fabry–Pérot cavity with mirrors of the sapphire/GaN interface and GaN/air interface. The epitaxial wafer with an RPG structure exhibits a narrower spectrum than with a normal structure; the linewidths are 26.1 nm and 37.5 nm, respectively. The emission ratio between the MQWs and the peak of the GaN layers was also larger in the RPG structure. The temperature-dependent emission characteristics of the epitaxial wafers with the two structures were measured from 10–300 K (spectra not shown here). The internal quantum efficiency was calculated as 50.6% and 31.8% for the two structures as $\eta_{\text{int}} = I_{300\text{K}}/I_{10\text{K}}$, where $I_{300\text{K}}$ and $I_{10\text{K}}$ are the integrated intensities at 300 K and 10 K, respectively. The much higher internal quantum efficiency and the smaller linewidth in the epitaxial wafer with the RPG structure demonstrate the high crystal quality of the active region. Typically, with an increase in the number of QW pairs, In-rich InGaN precipitates are more easily formed. The interfacial structure between InGaN and GaN can be deteriorated in InGaN/GaN MQWs, owing to the relaxation of the accumulated strain [53]. In the active region with the RPG structure, the growth was stopped temporarily after the first two QWs, and a 70-nm GaN spacing layer was inserted before the next two QWs, so that the stress accumulation was smaller than in the normal structure. With increasing excitation power, the linewidth of the spontaneous spectrum exhibited a sudden decrease, demonstrating the stimulated emission in the UVA band at room temperature in the epitaxial wafer with the RPG structure, as shown in Fig. 2b. However, this did not occur in the epitaxial wafer with a normal QW active region. This demonstrates the potential to develop UVA VCSELs using the InGaN active region with an RPG structure. A 355-nm YAG pulsed laser with a repetition frequency of 50 Hz and a pulse width of 20 ns was used in the stimulated emission measurement because a much higher excitation energy is required for stimulated emission in a bare epitaxial wafer. The interference pattern of the spectra in Fig. 2b is not as clear as Fig. 2a. This is because that the diameter of YAG excitation laser spot on the epitaxial wafer surface is ~2 mm, which is much larger than 70 μm. A larger area is excited and the interference between the surface of GaN/air and GaN/sapphire can be weakened.

Owing to the very short single-pass gain area in VCSELs, the coupling condition between the optical field inside the cavity and the active layers greatly influences the device performance. The coupling condition can be described by the gain enhancement factor Γ_r, which is determined by the spatial overlap of the optical field and the active region. Γ_r is calculated as:

$$\Gamma_r = \frac{L}{d_a}\frac{\int_{d_a}|E(z)|^2 dz}{\int_L |E(z)|^2 dz} \quad (1)$$

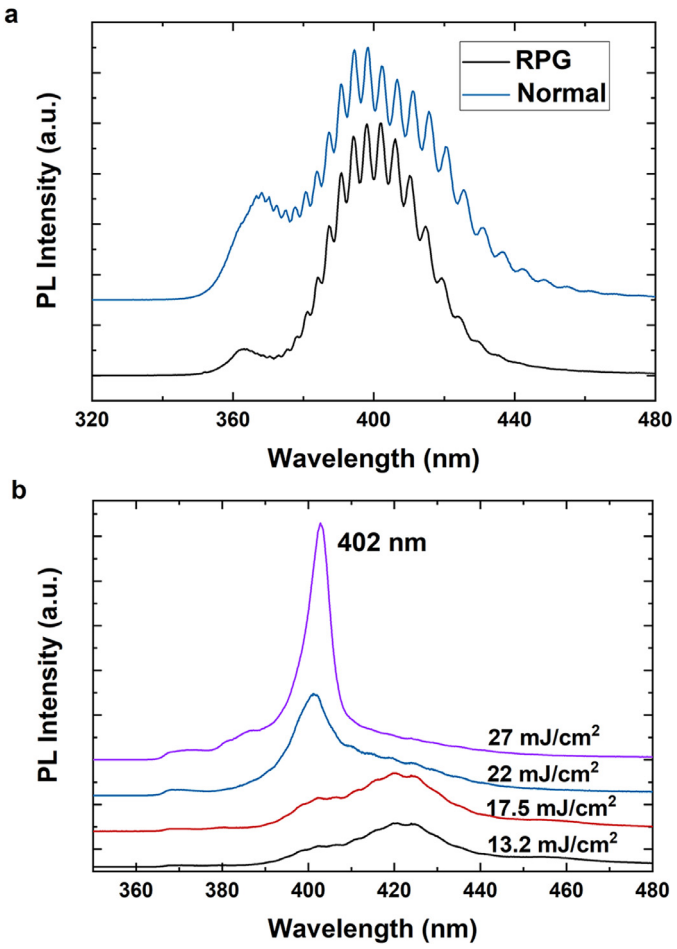

Fig. 2. Emission property of the epitaxial wafer. (a) Normalized PL spectra of epitaxial wafers with active region of RPG structure and normal structure; (b) PL spectra of epitaxial wafer with RPG structure at different excitation levels

where L, d_a, and $E(z)$ are the cavity length, thickness of the active region, and optical field standing wave pattern, respectively. In VCSELs, a larger gain enhancement factor means a stronger interaction between electrons and photons; the emission rate of the cavity mode can be boosted by the cavity effect. The emission can be strongly enhanced with well-coupled optical modes (active region overlaps with the antinode of the standing-wave pattern), whereas the emission is greatly suppressed with weak coupled optical modes (active region overlaps with the node of the standing-wave pattern). Accordingly, the threshold of the VCSEL is affected by the gain enhancement factor, calculated as:

$$g_{th} = \alpha_a + \frac{1}{\Gamma_r}\alpha_i\left(\frac{1}{\xi} - 1\right) + \frac{1}{\Gamma_r}\frac{1}{\xi L}\ln\frac{1}{R} \quad (2)$$

where α_a, α_i, and R are the loss in the active layer, loss in other layers, and mirror reflectivity, respectively. $\xi = d/L$, where d and L are the thicknesses of the active layer and the cavity, respectively. From the equation, it is clear that Γ_r has a significant influence on the threshold gain of VCSELs, especially when the thickness of the active region is small. The threshold of VCSELs can be effectively reduced by enhancing the coupling between the active layers and the optical field. In this study, an epitaxial wafer with an RPG structure is specially designed to enable different groups of QWs located at two adjacent antinodes of the standing wave inside the cavity to increase the coupling between the active region and the optical field to obtain a larger Γ_r. To explore the optical field distribution, we calculated the standing wave pattern of a 400-nm resonant mode in the VCSELs with active regions with the RPG structure and normal structure using the transfer matrix method, as shown in Fig. 3a, b; Γ_r was 1.8 and 1.4 for the two structures, respectively. Moreover, the loss of carriers through spontaneous emission was considerably reduced because the spacer medium around the nodes of the optical field contained no free carriers [54]. Thus, a lower threshold and higher power efficiency were expected in VCSELs with an RPG structure.

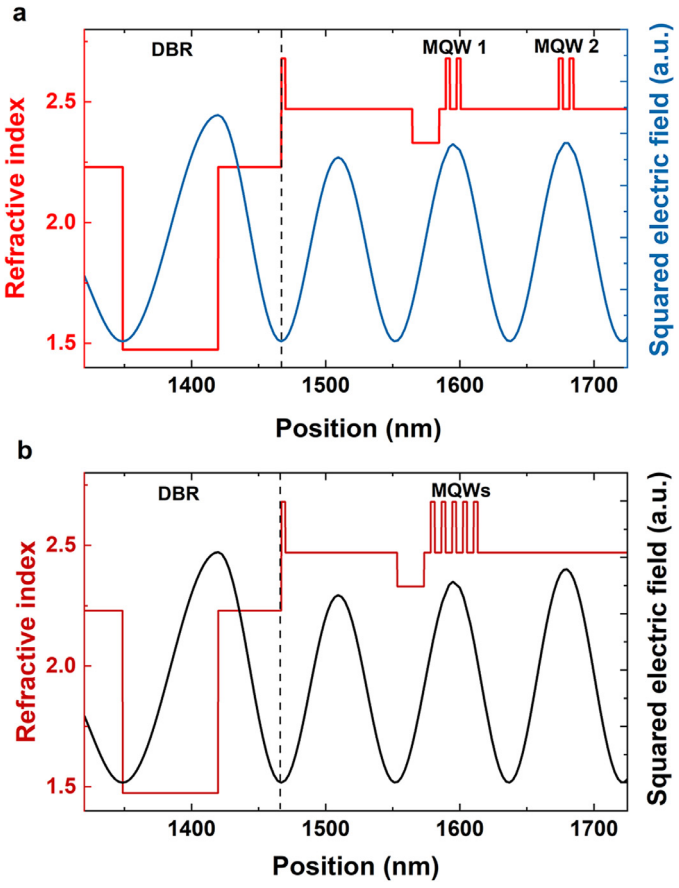

Fig. 3. Optical field distribution in VCSELs with different active regions. (a) RPG structure; (b) normal structure.

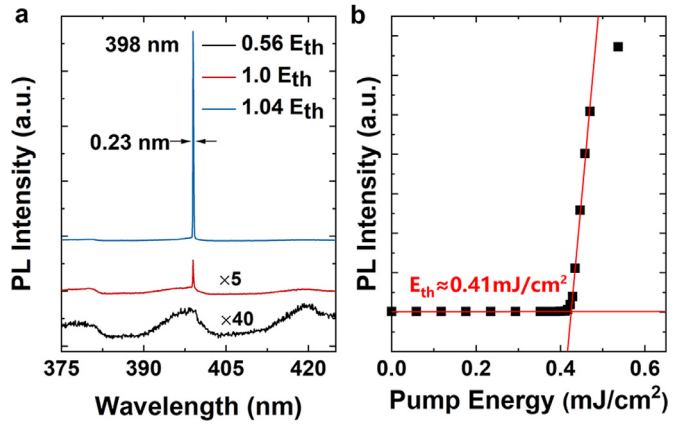

Fig. 4. Lasing characteristics of the UVC VCSEL. (a) Emission spectra of VCSEL with different excitation levels; the black and red curves are magnified by 40 times and 5 times, respectively, for clarity; (b) output intensity of VCSEL as a function of excitation energy

The fabricated UVA VCSEL with an RPG structure and a wedge-shaped cavity was optically excited in the same conditions as for PL measurement of the epitaxial wafers. Fig. 4a shows the emission spectra at different excitation levels measured from the same position of the VCSEL chip. The spectra with low excitation levels are enlarged for clarity; several weak peaks attributed to the spontaneous emission of the cav-

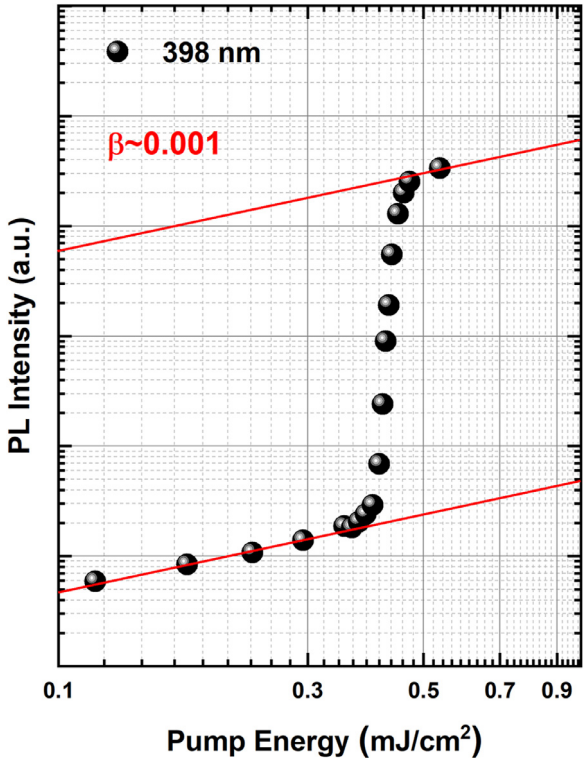

Fig. 5. Output intensity of VCSEL as a function of excitation energy. The data is plotted in double logarithm coordinates to show the typical "S" shaped curve for lasing action.

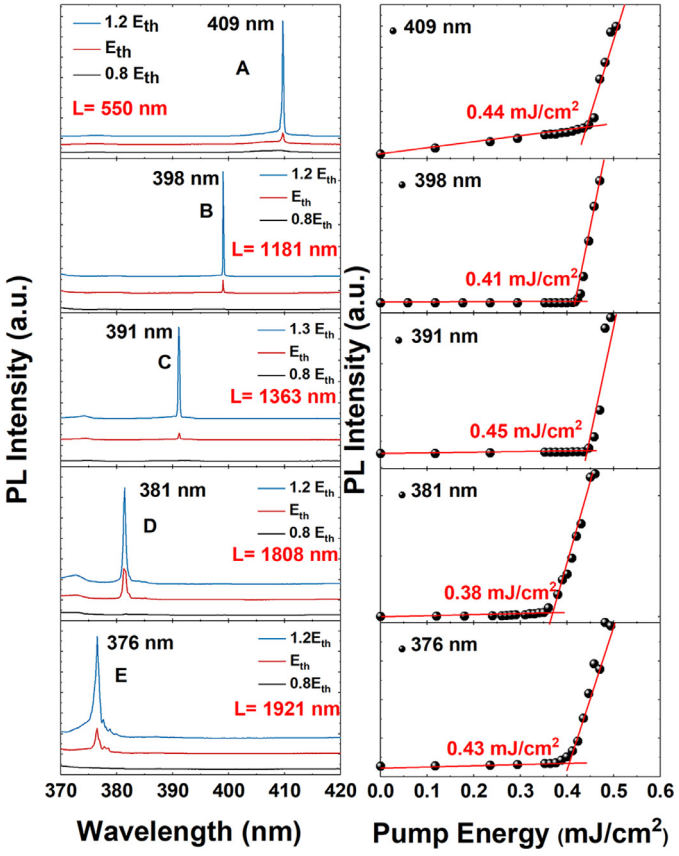

Fig. 6. Lasing spectra and the corresponding threshold characteristics of UVA VCSELs emitting at points. Point A (409 nm), point B (398 nm), point C (391 nm), point D (381 nm), point E (376 nm).

ity modes can be distinguished. The mode spacing λ_{FSR} was ~20 nm, and the effective cavity length L at this measured point was 1181 nm, calculated as:

$$L = \frac{\lambda_0^2}{2\left[n - (\frac{dn}{d\lambda})\lambda_0\right]\lambda_{FSR}} \quad (3)$$

where n is the refractive index at the emission wavelength λ_0 (398 nm); $dn/d\lambda$ is its dispersion, and λ_{FSR} is the mode spacing. With increasing excitation energy, a narrow peak emerges at 398 nm in the UVA band and increases significantly when the excitation energy exceeds the threshold. The linewidth of the cavity mode shows a sharp decrease from 5.6 to 0.23 nm, demonstrating the lasing action. Fig. 4b shows the output intensity as a function of excitation energy. The threshold energy density was fitted as 0.41 mJ/cm^2, corresponding to a threshold power density of 411 kW/cm^2, which is a low value for UV VCSELs. The output intensity as a function of the excitation energy plotted in double logarithm coordinates is shown in Fig. 5. The typical "S" shape of the output behavior demonstrates the lasing action; the spontaneous coupling factor (β) is ~0.001.

In EELs, the lasing wavelength is usually determined by the active region. Active layers with different alloy contents are required for devices working at different wavelengths. However, the resonant wavelength of the cavity mode of VCSELs can be modulated by the cavity length owing to the relatively short cavity. Changing the cavity length shifts the resonating wavelength and the optical field in the cavity. Eventually, the gain enhancement factor and the lasing wavelength can be adjusted for devices with different cavity lengths, as long as the gain spectrum of the active region can cover a wide spectral range. In this study, the emission of a single VCSEL chip can be tuned in a large range in the UVA band, benefiting from the wedge-shaped cavity. Fig. 6 shows the lasing spectra and the corresponding threshold characteristics of the UVA VCSELs measured at several different positions (points A–E) along the surface of a single VCSEL sample. The lasing wavelength obtained at point A was 409 nm, and the threshold energy density was ~0.49 mJ/cm^2. The effective cavity length of point A is ~550 nm, as calculated from the mode spacing. With increasing cavity length, the lasing peak was tuned to 398 nm, 391 nm, 381 nm, and 376 nm for points B–E, respectively. The corresponding cavity lengths were 1181 nm, 1363 nm, 1808 nm, and 1921 nm. The spacing between the measured points was ~1 mm, and the threshold energy densities were 0.41, 0.45, 0.39, and 0.43 mJ/cm^2, respectively. Because of the large differences in cavity length, the lasing modes at these points are belong to different longitudinal resonate order. The RPG structure in the epitaxial wafer used in this study was designed for cavity modes at ~400 nm to enable the separated QWs located at two adjacent antinodes of the standing wave. With different lasing wavelengths, the field distribution inside the cavity varies owing to the phase shift, which may influence the coupling between the optical field and the active region. To estimate this effect, the field distribution of the tunable lasing modes at different wavelengths was calculated, as shown in Fig. 7. When the lasing wavelength deviates from 400 nm, the antinodes of the mode field drift gradually from the active region; the mismatch increases with the deviation in the mode wavelength from 400 nm. However, in the tuning range of 376–409 nm in this study, the mismatch between the active region and the mode field is not large and can guarantee effective coupling of electrons and photons.

The VCSELs show tunable lasing spectra. Fig. 8a shows the normalized lasing spectra of points A–E on a single VCSEL chip. Low-threshold lasing extends from 376–409 nm, and a substantial proportion of the UVA band below the band gap of GaN can be covered. Using the modulation effect of the cavity length, wavelength-tunable UVA VCSELs were realized without the need to grow different active layers, which is much simpler than fabricating EELs. The linewidth of the UVA VCSELs at different wavelengths and the reflection spectrum of the top DBR are illustrated in Fig. 8b. The full width at half maximum (FWHM) of the lasing peak broadens monotonically from 0.22 nm to 0.53 nm when the peak

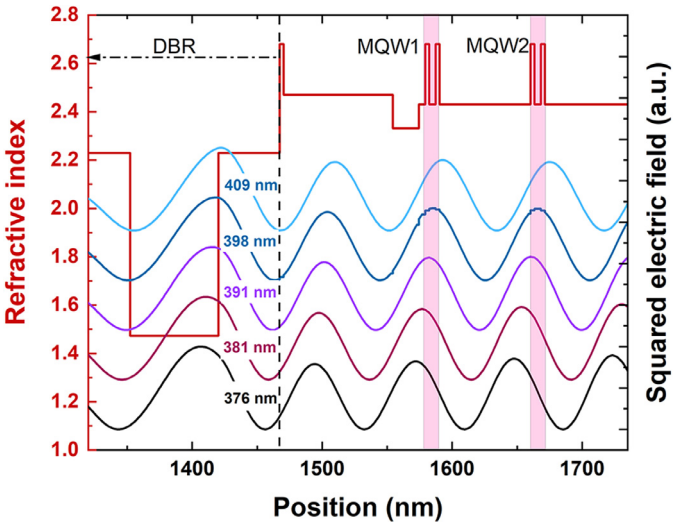

Fig. 7. Optical field distribution of tunable lasing modes with wavelengths of 376 nm, 381 nm, 391 nm, 398 nm, and 409 nm, respectively.

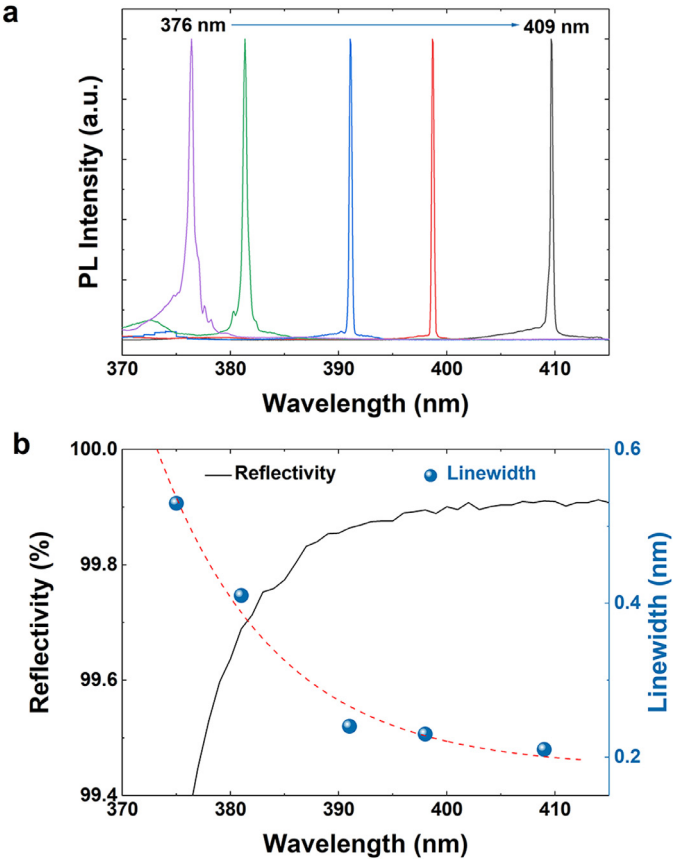

Fig. 8. Spectral characteristics of the tunable VCSELs. (a) Normalized lasing spectra of points A–E on a single VCSEL chip; (b) linewidth of lasing peak at different wavelengths (blue points) and reflectivity spectrum of top DBR (black curve)

wavelength decreases from 409 nm to 376 nm, which is likely due to the decrease in mirror reflectivity. Furthermore, the absorption loss caused by cavity layers is larger at shorter wavelengths, which may also cause broadening of the lasing peak. In the UVC VCSELs lasing at 275.9 nm fabricated in our previous study, the linewidth was larger (~0.78 nm), caused by large absorption losses [30].

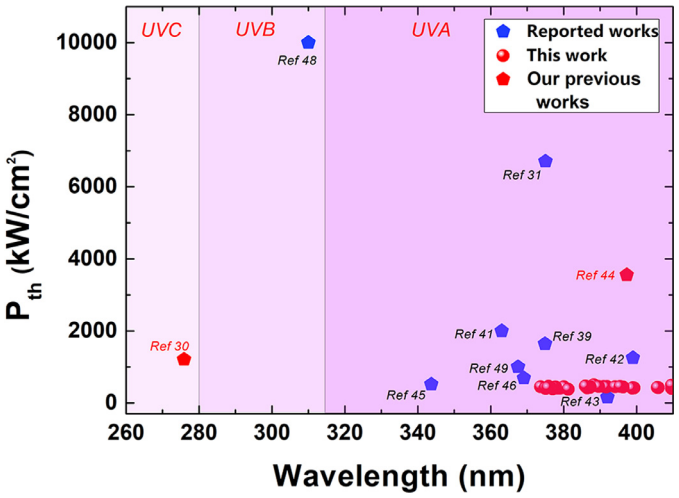

Fig. 9. Threshold power density as a function of lasing wavelength of reported UV VCSELs.

The threshold power density as a function of the lasing wavelength of the previously reported UV VCSELs is summarized in Fig. 9, along with the results reported in this study. The threshold power densities in this study ranged from 383–466 kW/cm^2, and were among the lowest values for UV VCSELs. The lasing wavelengths can cover a large part of the UV band below the GaN bandgap. The related physical mechanism can be attributed to: (1) the decrease in optical loss in the cavity; (2) the enhancement of optical–electronic coupling by the RPG structure with high crystal quality; and (3) the wavelength-tuning effect of the wedge-shaped cavity. The results and device design in this study are also promising for electrically injected UV VCSELs.

4. Conclusion

We have demonstrated low-threshold optically pumped UVA VCSELs with an RPG structure and a wedge-shaped cavity. Using the modulation effect of the cavity length, the lasing emission at different positions on a single VCSEL chip can be tuned from 376–409 nm, covering most of the UVA region below the GaN band gap. The threshold of the output intensity versus the pump energy, and the clear narrowing of the spectral linewidth demonstrate the lasing action. The threshold pumping power density ranges from 383–466 kW/cm^2, which are among the lowest values for UV VCSELs. Such low threshold lasing in the UVA band can be attributed to the RPG structure, the atomic-level flat cavity surface, and the high reflectivity of the dielectric DBRs. Furthermore, the device structure in this study holds potential for electrically injected UV VCSELs. This study is promising for the development of a small-footprint, power-efficient UV light source for atomic clocks, medical applications, and compact disinfection systems.

Declaration of Competing Interest

The authors declare that they have no conflicts of interest in this work.

Acknowledgments

This work was supported by the National Key Research and Development Program of China (Grants No. 2017YFE0131500 and 2016YFB0400803) and the National Natural Science Foundation of China (Grants No. U1505253 and 62104204).

References

[1] K. Iga, Forty years of vertical-cavity surface-emitting laser: Invention and innovation, Jpn. J. Appl. Phys. 57 (8S2) (2018) 08PA01-10.
[2] K. Iga, Vertical-cavity surface-emitting laser: its conception and evolution, Jpn. J. Appl. Phys. 47 (1) (2008) 1–10.
[3] J. Wu, H. Long, X. Shi, et al., Polariton lasing in InGaN quantum wells at room temperature, Opto-Electron, Adv. 2 (12) (2019) 19001401–19001405.
[4] C. Weisbuch, M. Nishioka, A. Ishikawa, et al., Observation of the coupled exciton-photon mode splitting in a semiconductor quantum microcavity, Phys. Rev. Lett. 69 (23) (1992) 3314–3317.
[5] L.M. Giovane, J. Wang, M.V.R. Murty, et al., Development of Next Generation Data Communication VCSELs, in: Optical Fiber Communication Conference (OFC) 2020, 10, 1364, 2020, p. M3D.5.
[6] G. Zhao, J. Yang, E. Hegblom, et al., Multi-junction VCSEL arrays with high performance and reliability for mobile and automotive 3D sensing applications, SPIE OPTO 11704 (2021) 117040A.
[7] T. Hanada, Basic properties of ZnO, GaN, and related materials. Oxide and nitride semiconductors, Springer, 2009.
[8] W.W. Bi, H.H. Kuo, P. Ku, et al., Handbook of GaN Semiconductor Materials and Devices, CRC Press, 2017.
[9] T.C. Lu, C.C. Kao, H.C. Kuo, et al., CW lasing of current injection blue GaN-based vertical cavity surface emitting laser, Appl. Phys. Lett. 92 (14) (2008) 141102.
[10] T. Furuta, K. Matsui, K. Horikawa, et al., Room-temperature CW operation of a nitride-based vertical-cavity surface-emitting laser using thick GaInN quantum wells, Jpn. J. Appl. Phys. 55 (2016) 5S 05FJ11-01-04.
[11] T. Hamaguchi, Y. Hoshina, K. Hayashi, et al., Room-temperature continuous-wave operation of green vertical-cavity surface-emitting lasers with a curved mirror fabricated on {20– 21} semi-polar GaN, Appl. Phys. Express 13 (2020) 041002 4..
[12] T. Hamaguchi, H. Nakajima, M. Tanaka, et al., Sub-milliampere-threshold continuous wave operation of GaN-based vertical-cavity surface-emitting laser with lateral optical confinement by curved mirror, Appl. Phys. Express 12 (2019) 044004 4..
[13] S. Izumi, N. Fuutagawa, T. Hamaguchi, et al., Room-temperature continuous-wave operation of GaN-based vertical-cavity surface-emitting lasers fabricated using epitaxial lateral overgrowth, Appl. Phys. Express 8 (6) (2015) 062702.
[14] M. Kuramoto, S. Kobayashi, T. Akagi, et al., Watt-class blue vertical-cavity surface-emitting laser arrays, Appl. Phys. Express 12 (9) (2019) 091004.
[15] M. Kuramoto, S. Kobayashi, T. Akagi, et al., High output power and high temperature operation of blue GaN-based vertical-cavity surface-emitting laser, Appl. Phys. Express 11 (11) (2018) 112101.
[16] Y. Mei, G.E. Weng, B.P. Zhang, et al., Quantum dot vertical-cavity surface-emitting lasers covering the 'green gap, Light Sci. Appl. 6 (1) (2017) e16199.
[17] G. Weng, Y. Mei, J. Liu, et al., Low threshold continuous-wave lasing of yellow–green InGaN-QD vertical-cavity surface-emitting lasers, Opt. Express 24 (14) (2016) 15546–15553.
[18] H. Xu, Y. Mei, R. Xu, et al., Green VCSELs based on nitride semiconductors, Jpn. J. Appl. Phys. 59 (2020) 1–9 SO0803..
[19] T.C. Lu, S.W. Chen, T.T. Wu, et al., Continuous wave operation of current injected GaN vertical cavity surface emitting lasers at room temperature, Appl. Phys. Lett. 97 (7) (2010) 071114.
[20] D. Kasahara, D. Morita, T. Kosugi, et al., Demonstration of blue and green GaN-based vertical-cavity surface-emitting lasers by current injection at room temperature, Appl. Phys. Express 4 (7) (2011) 072103.
[21] G. Cosendey, A. Castiglia, G. Rossbach, et al., Blue monolithic AlInN-based vertical cavity surface emitting laser diode on free-standing GaN substrate, Appl. Phys. Lett. 101 (15) (2012) 151113.
[22] C. Holder, J.S. Speck, S.P. DenBaars, et al., Demonstration of nonpolar GaN-based vertical-cavity surface-emitting lasers, Appl. Phys. Express 5 (9) (2012) 092104.
[23] T. Onishi, O. Imafuji, K. Nagamatsu, et al., Continuous wave operation of GaN vertical cavity surface emitting lasers at room temperature, IEEE J. Quantum Electron. 48 (9) (2012) 1107–1112.
[24] C. Holder, J. Leonard, R. Farrell, et al., Nonpolar III-nitride vertical-cavity surface emitting lasers with a polarization ratio of 100% fabricated using photoelectrochemical etching, Appl. Phys. Lett. 105 (3) (2014) 031111.
[25] W.J. Liu, X.L. Hu, L.Y. Ying, et al., Room temperature continuous wave lasing of electrically injected GaN-based vertical cavity surface emitting lasers, Appl. Phys. Lett. 104 (25) (2014) 251116.
[26] M. Kuramoto, S. Kobayashi, T. Akagi, et al., Nano-height cylindrical waveguide in GaN-based vertical-cavity surface-emitting lasers, Appl. Phys. Express 13 (8) (2020) 082005.
[27] K. Terao, H. Nagai, D. Morita, et al., Blue and green GaN-based vertical-cavity surface-emitting lasers with AlInN/GaN DBR, Proceeding of SPIE, 2021.
[28] H.C. Yu, Z.W. Zheng, Y. Mei, et al., Progress and prospects of GaN-based VCSEL from near UV to green emission, Prog. Quantum Electron. 57 (2018) 1–19.
[29] T.C. Hsu, Y.T. Teng, Y.W. Yeh, et al., Perspectives on UVC LED: Its Progress and Application, Photonics 8 (6) (2021).
[30] Z. Zheng, Y. Mei, H. Long, et al., AlGaN-Based Deep Ultraviolet Vertical-Cavity Surface-Emitting Laser, IEEE Electron Device Lett 42 (3) (2021) 375–378.
[31] Y.J. Park, T. Detchprohm, K. Mehta, et al., Optically pumped vertical-cavity surface-emitting lasers at 375 nm with air-gap/Al0:05Ga0:95N distributed Bragg reflectors, in: Proc. SPIE, Vertical-Cavity Surface-Emitting Lasers XXIII, 2019.
[32] J.H. Jeon, M.G. Kim, H.S. Lee, Phototactic behavior 4: Attractive effects of Trialeurodes vaporariorum adults to light-emitting diodes under laboratory conditions, J. Korean Soc. Appl. Biol. Chem. 57 (2) (2014) 197–200.
[33] P.O. Nyangaresi, Y. Qin, G. Chen, et al., Effects of single and combined UV-LEDs on inactivation and subsequent reactivation of E. coli in water disinfection, Water Res 147 (2018) 331–341.
[34] P.O. Nyangaresi, Y. Qin, G. Chen, et al., Comparison of UV-LED photolytic and UV-LED/TiO2 photocatalytic disinfection for Escherichia coli in water, Catal. Today 335 (2019) 200–207.
[35] D.-K. Kim, D.-H. Kang, UVC LED Irradiation Effectively Inactivates Aerosolized Viruses, Bacteria, and Fungi in a Chamber-Type Air Disinfection System, Appl. Environ. Microbiol. 84 (17) (2018) e00944-00918.
[36] S. Zhang, H. Li, X. Wang, et al., Highly Integrated In Situ Photoenergy Gas Sensor with Deep Ultraviolet LED, ACS Omega 5 (17) (2020) 9985–9990.
[37] S.F. Shiba, J. Beavers, D. Laramore, et al., UV-LED Lithography System and Characterization, in: 2020 IEEE 15th International Conference on Nano/Micro Engineered and Molecular System (NEMS), 1109, 2020, pp. 73–76. 10.
[38] J. Rass, N.Lobo Ploch, Nitride-Based UV-LEDs and Their Application 11 (3) (2016) 36–40.
[39] Y.S. Liu, A.F.M. Saniul Haq, K. Mehta, et al., Optically pumped vertical-cavity surface-emitting laser at 374.9 nm with an electrically conducting n-type distributed Bragg reflector, Appl. Phys. Express 9 (11) (2016) 111002.
[40] Y. Chao, W. Tang, X. Wang, Properties of Resistivity, Reflection and Absorption Related to Structure of ITO Films, J. Mater. Sci. Technol. 28 (4) (2012) 325–328.
[41] J.M. Redwing, D.A.S. Loeber, N.G. Anderson, et al., An optically pumped GaN–AlGaN vertical cavity surface emitting laser, Appl. Phys. Lett. 69 (1) (1996) 1–3.
[42] T. Someya, R. Werner, A. Forchel, et al., Room Temperature Lasing at Blue Wavelengths in Gallium Nitride Microcavities, Science 285 (17) (1999) 1905–1906.
[43] S.H. Park, J. Kim, H. Jeon, et al., Room-temperature GaN vertical-cavity surface-emitting laser operation in an extended cavity scheme, Appl. Phys. Lett. 83 (11) (2003) 2121–2123.
[44] J.Y. Zhang, L.E. Cai, B.P. Zhang, et al., Blue-Violet Lasing of Optically Pumped GaN-Based Vertical Cavity Surface-Emitting Laser With Dielectric Distributed Bragg Reflectors, J. Lightwave Technol. 27 (1) (2009) 55–59.
[45] R. Chen, H.D. Sun, T. Wang, et al., Optically pumped ultraviolet lasing from nitride nanopillars at room temperature, Appl. Phys. Lett. 96 (24) (2010) 241101.
[46] A. Faraon, W. Zhou, F. Koyama, et al., GaN vertical-cavity surface-emitting laser with a high-contrast grating reflector, in: Proc. SPIE, High Contrast Metastructures VII, 2018.
[47] C. Zhang, R.T. El Afandy, J. Zhang, et al., Development of nanopore-based near ultraviolet vertical-cavity surface emitting lasers, in: Proc. SPIE, Gallium Nitride Materials and Devices XIV, 2019.
[48] F. Hjort, J. Enslin, M. Cobet, et al., A 310 nm Optically Pumped AlGaN Vertical-Cavity Surface-Emitting Laser, ACS Photonics 8 (1) (2021) 135–141.
[49] Y.-S. Liu, A.F.M.S. Haq, T.-T. Kao, et al., Development for Ultraviolet Vertical Cavity Surface Emitting Lasers, in: European Conference on Lasers and Electro-Optics - European Quantum Electronics Conference, 2015, p. PDA2.
[50] G. Weng, S. Chen, Y. Mei, et al., Multiwavelength GaN-Based Surface-Emitting Lasers and Their Design Principles, Ann. Phys. 532 (1) (2019) 1900308.
[51] Y. Mei, Y.H. Chen, L.Y. Ying, et al., High Q factor Electrically Injected Green Micro Cavity, J. Lightwave Technol. 39 (9) (2021) 2895–2901.
[52] W.J. Liu, S.Q. Chen, X.L. Hu, et al., Low Threshold Lasing of GaN-Based VCSELs With Sub-Nanometer Roughness Polishing, IEEE Photonics Technol. Lett. 25 (20) (2013) 2014–2017.
[53] D.J. Kim, Y.T. Moon, K.M. Song, et al., Structural and optical properties of InGaN/GaN multiple quantum wells: The effect of the number of InGaN/GaN pairs, J. Cryst. Growth 221 (1) (2000) 368–372.
[54] M.Y.A. Raja, S.R.J. Brueck, M. Osinski, et al., Resonant periodic gain surface-emitting semiconductor lasers, IEEE J. Quantum Electron. 25 (6) (1989) 1500–1512.

Yang Mei was born in Henan, China, in 1994. He received the B.S. degree in physics from the China University of Geoscience, Wuhan, China, in 2014 and the Ph.D. degree from Xiamen University, Xiamen, China, in 2020. He is currently an Assistant Professor with the College of Electronic Science and Technology, Xiamen University, where he is engaged in wide gap semiconductor materials and devices, especially GaN-based microcavities and vertical-cavity surface-emitting lasers.

Bao-Ping Zhang was born in Hebei, China, in 1963. He received the B.S. degree in physics from Lanzhou University, Lanzhou, China, in 1983, the M.E. degree in microelectronics from Hebei Semiconductor Research Institute, Shijiazhuang, China, and the Dr. Eng. degree in applied physics from the University of Tokyo, Tokyo, Japan, in 1994. He is currently a Distinguished Professor with the School of Electronic Science and Engineering, Xiamen University, China, where he is engaged in wide gap semiconductor materials and devices, especially GaN-based LEDs and vertical-cavity surface-emitting lasers (VCSELs).